Title

Differentiating Luminal and Membrane-Associated Nuclear Envelope Proteins

Journal

Biophysical Journal, 118(10)

ISSN

0006-3495

Authors

Hennen, Jared

Kohler, John

Karuka, Siddarth Reddy

et al.

Publication Date

2020-05-01

DOI

10.1016/j.bpj.2020.03.025

Peer reviewed

Biophysical Journal
Article

Biophysical Society

Differentiating Luminal and Membrane-Associated Nuclear Envelope Proteins

Jared Hennen,[1] John Kohler,[1] Siddarth Reddy Karuka,[1] Cosmo A. Saunders,[2] G. W. Gant Luxton,[2] and Joachim D. Mueller[1,3,*]

[1]School of Physics and Astronomy, [2]Department of Genetics, Cell Biology, and Development, and [3]Department of Biomedical Engineering, University of Minnesota, Minneapolis, Minnesota

ABSTRACT The nuclear envelope (NE) consists of two concentric nuclear membranes separated by the lumen, an ~40-nm-wide fluid layer. NE proteins are implicated in important cellular processes ranging from gene expression to nuclear positioning. Although recent progress has been achieved in quantifying the assembly states of NE proteins in their native environment with fluorescence fluctuation spectroscopy, these studies raised questions regarding the association of NE proteins with nuclear membranes during the assembly process. Monitoring the interaction of proteins with membranes is important because the binding event is often associated with conformational changes that are critical to cellular signaling pathways. Unfortunately, the close physical proximity of both membranes poses a severe experimental challenge in distinguishing luminal and membrane-associated NE proteins. This study seeks to address this problem by introducing new, to our knowledge, fluorescence-based assays that overcome the restrictions imposed by the NE environment. We found that luminal proteins violate the Stokes-Einstein relation, which eliminates a straightforward use of protein mobility as a marker of membrane association within the NE. However, a surprising anomaly in the temperature-dependent mobility of luminal proteins was observed, which was developed into an assay for distinguishing between soluble and membrane-bound NE proteins. We further introduced a second independent tool for distinguishing both protein populations by harnessing the previously reported undulations of the nuclear membranes. These membrane undulations introduce local volume changes that produce an additional fluorescence fluctuation signal for luminal, but not for membrane-bound, proteins. After testing both methods using simple model systems, we apply the two assays to investigate a previously proposed model of membrane association for the luminal domain of SUN2, a constituent protein of the linker of nucleoskeleton and cytoskeleton complex. Finally, we investigate the effect of C- and N-terminal tagging of the luminal ATPase torsinA on its ability to associate with nuclear membranes.

SIGNIFICANCE Protein association with membranes has been shown to be important in the regulation of cell signaling and the assembly of protein complexes. However, identifying the presence or absence of membrane binding for nuclear envelope (NE) proteins is experimentally challenging because the two nuclear membranes are only separated by an ~40 nm fluid layer called the lumen. This work overcomes this obstacle by developing two assays that experimentally distinguish luminal and membrane-associated NE proteins. These methods provide insight into membrane interactions during assembly and identify the effect of labeling of NE proteins on membrane association, as demonstrated by the results obtained for linker of nucleoskeleton and cytoskeleton complex protein SUN2 and the luminal ATPase torsinA.

INTRODUCTION

The nuclear envelope (NE) is a specialized subdomain of the endoplasmic reticulum (ER) that physically segregates the contents of the nucleoplasm from that of the cytoplasm as well as controls genome organization and gene expression (1). It consists of the concentric inner and outer nuclear membranes (INM and ONM, respectively), which are separated by a lumen known as the perinuclear space. Mutations in genes encoding proteins found within the NE—such as the ONM nesprin proteins and INM Sad1/UNC-84 domain protein 2 (SUN2), which interact within the lumen to form the linker of nucleoskeleton and cytoskeleton (LINC) complex (2)—cause a wide spectrum of diseases (3). The genetics and clinical phenotypes of these diseases have been carefully documented, but the cellular and molecular mechanisms responsible for their pathophysiology remain unclear, despite this

Submitted January 3, 2020, and accepted for publication March 27, 2020.

*Correspondence: jochen@umn.edu

Editor: Jason Swedlow.

https://doi.org/10.1016/j.bpj.2020.03.025

information being essential for the development of novel treatments.

We recently established fluorescence fluctuation spectroscopy (FFS) and time-shifted mean-segmented Q (tsMSQ) analysis (Fig. S1) for studying protein complex assembly in the NE of living cells (4,5). These techniques harness fluctuations in the fluorescence intensity signal from fluorescently labeled proteins, allowing for the characterization of protein dynamics within living cells (5). In particular, tsMSQ analysis had previously been shown to identify the oligomeric state and mobility of proteins within living cells (4). Using these techniques, we reported the formation of SUN2 trimers in vivo (6), in agreement with previous in vitro biochemical, computational, and structural studies of SUN2 (7–10). Intriguingly, we observed that mobility of the SUN2 luminal domain was significantly reduced upon homotrimerization (4,5). We hypothesized that the SUN2 luminal domain homotrimers become membrane associated through their ability to interact with endogenous nesprins present at the ONM, whereas monomers of the SUN2 luminal domain cannot interact with nesprins and therefore remain soluble in the NE lumen. However, we were unable to experimentally test this hypothesis because of the absence of a method for distinguishing between luminal and membrane-associated proteins within the NE of living cells.

The association of proteins with membranes has been shown to impact protein complex assembly, whether from conformational changes or an effective change in concentration (11,12). Thus, the identification of membrane association is critical to the development of models of assembly for protein complexes. Various fluorescence scanning and imaging techniques have been used to identify protein association with the plasma membrane and other cellular organelles (13,14). These techniques rely on optical resolution to distinguish membrane structures from the solvent surrounding them. The spatial separation of both nuclear membranes has been reported to be on the order of 40 nm (Fig. 1 *A*), which is below the resolution limit of fluorescence microscopy, making it impossible to distinguish luminal from membrane-associated proteins by conventional imaging methods. An alternative approach for identifying protein association with the plasma membrane, not based on optical resolution, utilizes the measurement of protein mobility by FFS. Binding of a cytoplasmic protein to the plasma membrane is associated with a significant reduction of translational diffusional mobility, which is experimentally detected by the fluorescence autocorrelation function (15). Because the mobility of luminal proteins has not yet been investigated, we explored the dependence of translational diffusion on molecular mass and found it to be inconsistent with the Stokes-Einstein relation. This deviation between theory and experiment was modeled by including near-wall effects on the process of diffusion in the lumen. Our data and model demonstrate that experimental mobility is a poor marker of membrane association at the NE.

Luminal proteins are also affected by the presence of undulations in the distance separating both membranes (Fig. 1 *B*), as was shown recently (4). These undulations introduce slow changes in the local volume that contribute to the measured fluctuations in the fluorescence signal of luminal proteins (Fig. 1 *C*). In contrast, the signal of membrane-bound proteins is unaffected by the local volume changes (Fig. 1 *C*; (4)). This observation motivated further characterization of the membrane undulations to establish assays for differentiating luminal and membrane-associated protein populations. Specifically, we investigated the temperature dependence of the membrane undulations in conjunction with protein mobility, which led to the development of an assay for distinguishing between both protein populations. In addition, we established a second, independent assay that utilizes the cross-correlation signal between the green-labeled target protein and a red-fluorescing luminal protein, which acts as a reference marker. These two methods provide an important cross-check to validate experimental results with two independent assays.

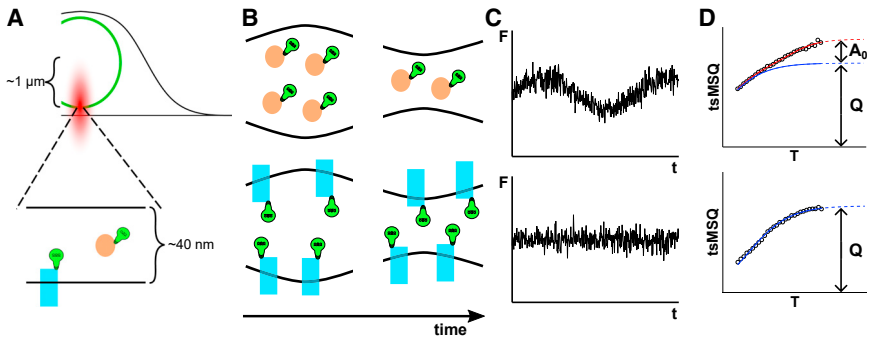

FIGURE 1 Membrane-bound and luminal proteins in the presence of local volume fluctuations at the NE. (*A*) Because the two-photon PSF (*red oval*) is significantly wider than the NE, EGFP-tagged membrane-associated (*blue*) and luminal (*orange*) NE proteins cannot be distinguished optically. (*B*) Nuclear membrane undulations introduce fluctuations in the local NE volume, which alter the number of luminal EGFP-tagged proteins illuminated by the PSF (*top*) without affecting the number of membrane-bound proteins illuminated (*bottom*). (*C*) These local NE volume changes give rise to an additional fluctuation in the fluorescence intensity signal generated by EGFP-tagged luminal NE proteins, as indicated by the exaggerated sinusoidal variation in the signal plotted in the top graph. In contrast, the local NE volume changes have no effect on the signal generated by EGFP-tagged membrane-associated NE proteins (*bottom*). (*D*) tsMSQ analysis accounts for the diffusion process of membrane-associated proteins and identifies their Q amplitude (*bottom*). tsMSQ analysis of luminal NE proteins requires the diffusional term and an additional exponential correlation process with amplitude A_0 to account for the slow intensity variations observed because of the local changes in NE volume (*top*). To see this figure in color, go online.

After experimental verification of both methods with model protein systems, we applied each technique to proteins of biological interest. First, we addressed the question raised above, whether the luminal domain of SUN2 exists as a mixture of luminal monomers and nuclear-membrane-associated trimers. Second, we studied the membrane association of torsinA, a luminal member of the ATPases associated with various cellular activities (AAA+) protein family implicated in the regulation of LINC complex assembly (16). Specifically, we investigated whether fusing EGFP to the N-terminus or C-terminus of torsinA on its ability to associate with nuclear membranes. Identifying the extent of membrane association of luminal proteins during the assembly process provides information critical to the development of accurate models of protein complex assembly. Thus, we anticipate that these methods will enable future mechanistic investigations of the impact of human disease-associated genetic mutations on the assembly and function of NE proteins.

MATERIALS AND METHODS

Sample preparation

All measurements were performed in U2OS cells (ATCC, Manassas, VA) maintained in Dulbecco's modified Eagle's medium with 10% fetal bovine serum (Thermo Fisher Scientific, Waltham, MA). For most experiments, cells were transferred into eight-well plates with No. 1.5H glass bottoms (Cellvis, Mountain View, CA) before transfection. For the temperature-controlled experiments, cells were transferred into six-well plates containing No. 1.5 glass coverslips (Thermo Fisher Scientific) in preparation for their use in a CherryTemp microfluidic temperature controller (Cherry Biotech, Rennes, France). Transient transfection was performed using GenJet (SignaGen Laboratories, Rockville, MD) 12–24 h before measurement according to the instructions provided by the manufacturer. Immediately before measurements were performed, the growth medium was replaced with Dulbecco's phosphate-buffered saline containing calcium and magnesium (Biowhittaker, Walkerville, MD). Measurements in the presence of sodium azide and 2-deoxyglucose were performed 30 min after adding solution containing 0.02% azide and 5 mM 2-deoxyglucose. Measurements in the presence of nocodazole were performed 3 h after adding solution containing 10 mM nocodazole.

DNA constructs

The cDNA constructs encoding SS-Venus, SS-Venus$_3$, SS-Venus$_4$, SS-Venus$_5$, or SS-Venus$_6$ were generated as follows. Briefly, we first obtained the previously described pVenus (V)-N1-derived VN1, VV, VVV, VVVV, VVVVV, and VVVVVV (respectively referred to as Venus, Venus$_2$, Venus$_3$, Venus$_4$, Venus$_5$, and Venus$_6$ in this work) cDNA constructs (17) as a generous gift from Dr. Stephen S. Vogel (National Institute on Alcohol Abuse and Alcoholism, Rockville, MD). These constructs contain increasing numbers of Venus harboring the A206K mutation that inhibits the intrinsic dimerization of wild-type (WT) Venus (18). We fused the signal sequence (SS) of the luminal protein torsinA to the 5′ end of the first Venus by PCR using the primers SS-Venus-F (5′-CTGCTGCTGGC GCCGTCCGTGGTGCAGGCGGTGAGCAAGGGCGAGG-3′) and SS-Venus-R (5′-CAGGCCCAGCACGGCCCGGCCCAGCTTCATGGTGGC GACCGGTAGC-3′). Each construct was subsequently validated by sequencing at the University of Minnesota Genomics Center. The previously described cDNA construct encoding torsinA-mGFP (19), referred to as SS-torsinA^{WT}-EGFP in this work, was a generous gift from Dr. Phyllis I. Hanson (University of Michigan, Ann Arbor, MI). The generation of the cDNA constructs encoding EGFP, SS-EGFP, SS-EGFP-KASH2^{WT}, SS-EGFP-torsinA$^{NTD\text{-}2\times Leu}$, HRas-EGFP, SS-mCherry-KDEL, or SS-EGFP-SUN2$^{261–731}$ used in this work was previously described elsewhere (4,20,21).

Experimental setup

Measurements were performed on a home built two-photon microscope as previously described (22,23). A 63× C-Apochromat water-immersion objective with a 1.2 numerical aperture (Zeiss, Oberkochen, Germany) served to focus excitation light with a wavelength of 1000 nm, unless otherwise stated, and an average power after the objective of 0.3–0.4 mW. Emitted photons were detected using avalanche photodiodes (SPCM-AQR-14 APD; Perkin-Elmer, Dumberry, Quebec, Canada) and recorded with a Flex04-12D card (correlator.com, Bridgewater, NJ) sampled at 20 kHz before being analyzed with programs written in IDL 8.7 (Harris Geospatial Solutions, Boulder, CO). Z-scans were performed using a PZ2000 piezo stage (ASI, Eugene, OR) moved axially by an arbitrary waveform generator (model no. 33522A; Agilent Technologies, Santa Clara, CA). A linear ramp function was created by the generator with a peak-to-peak amplitude of 1.6 V, corresponding to 24.1 μm of axial travel, and a period of 10 s for a speed of 4.82 μm/s. Experiments requiring temperature manipulation were performed with a CherryTemp microfluidic temperature controller (Cherry Biotech). Dual-color measurements were performed with a dichroic mirror centered at 580 nm (FF580-FDi01; Semrock, Rochester, NY) used to split emitted light into two channels along with an additional 84-nm-wide bandpass filter centered at 510 nm (FF01-510/84; Semrock) placed in the green channel to remove any reflected mCherry fluorescence.

Measurement procedure

FFS measurements of the NE were performed as previously described (22). Briefly, cells expressing the proteins of interest were identified via wide-field epifluorescence microscopy. The two-photon point spread function (PSF) was focused laterally at the geometric center of the nucleus, and z-scans were performed to ensure the proper localization of expressed fluorescently labeled proteins to the NE (22). Next, the PSF was focused axially on the ventral NE by maximizing the detected fluorescence intensity, and a 60-s-long photon record was collected before repeating this process at the dorsal NE. When temperature was varied, measurements were performed within the same cells at each temperature value. Long-term effects on cells due to low temperature were minimized by keeping cells at each temperature for no more than 1 h. Calibration measurements were performed in the cytoplasm of cells expressing EGFP to determine its monomeric brightness λ_{EGFP}. Dual-color measurements were performed with the protein of interest tagged with EGFP while SS-mCherry-KDEL served as a monomeric luminal marker protein (20).

Analysis procedure

Single-color FFS data were analyzed using the previously described tsMSQ method (5,24). A detailed description of tsMSQ analysis, as well as code and sample data, can be found in Karuka et al. (25). The data obtained from the green and red channel were used to calculate tsMSQ$_{gg}$ and tsMSQ$_{rr}$, respectively. This was done by splitting the photon record for the green (k_g) or the red channel (k_r) into $n = T\backslash T_{seg}$ segments, where T is the total data acquisition time, T_{seg} is the segment time, and \ denotes integer division. The single-color tsMSQ is determined by (5)

$$\mathrm{tsMSQ_{jj}}\left(T_{seg}\right) = \frac{1}{n}\sum_{i=1}^{n}\frac{\left\langle \Delta k_j(t)\Delta k_j(t+\tau_s)\right\rangle_i}{\left\langle k_j\right\rangle_i} - 1, \qquad (1)$$

where j = g or r for the green or red channel, respectively; $\Delta k_j(t) = k_j(t) - \langle k_j \rangle$; and $\langle\rangle_i$ denotes averaging over the i^{th} segment. We performed bootstrapped tsMSQ analysis (24), fitting the data to previously described models of single-species diffusion, two-species diffusion, or single-species diffusion plus an exponential correlation (5). Unless otherwise stated, single-color measurements of fluorescently labeled NE proteins were performed at low intensities ($F_j < 60$ kHz). This simplified the analysis by allowing fits to be performed without including an exponential correlation term associated with nuclear membrane undulations, as this process was shown to be insignificant at these low intensities (24). The Q-values recovered from fits were then converted to normalized brightness b via the two equations $Q = \gamma_2 \lambda \tau_S$ and $b = \lambda/\lambda_{EGFP}$, where γ_2 is the PSF shape factor, λ is the brightness, and τ_S is the photon count sampling time.

Dual-color FFS data were analyzed utilizing the photon counts measured by both detection channels following a similar procedure as described above. We split both the green and red photon records into n segments and then calculated the amplitude of the cross-correlation tsMSQ by (20)

$$\mathrm{tsMSQ}_{\mathrm{gr}}\left(T_{\mathrm{seg}}\right) = \frac{1}{n}\sum_{i=1}^{n}\frac{\left\langle \Delta k_g(t)\Delta k_r(t+\tau_s)\right\rangle_i}{\left\langle k_g\right\rangle_i} \tag{2}$$

For this study, we consider the special case in which the EGFP- and the mCherry-labeled proteins are noninteracting. If both noninteracting proteins are luminal (denoted by subscript LL), their tsMSQ$_{\mathrm{gr}}$ curve is (20)

$$\mathrm{tsMSQ}^{(-)}_{\mathrm{gr,LL}}\left(T_{\mathrm{seg}}\right) = f_{\mathrm{ct}}\mathrm{tsMSQ}_{gg,D}\left(T_{\mathrm{seg}}\right) + \frac{F_r}{F_g}\mathrm{tsMSQ}_{gg,E}\left(T_{\mathrm{seg}}\right), \tag{3}$$

where $F_r = \langle k_r \rangle/\tau_S$ and $F_g = \langle k_g \rangle/\tau_S$ are the total fluorescence intensities detected by the red and green channel, respectively, and $F_{\mathrm{ct}} = F_{EGFP,r}/F_{EGFP,g}$ is the intensity fraction of spectral cross talk from EGFP into the red channel (20). In contrast, the spectral cross talk of mCherry into the green channel is effectively zero ($F_{\mathrm{mGh},g} \approx 0$) (26). tsMSQ$_{\mathrm{gg,X}}$ is the autocorrelation tsMSQ of the green channel as previously defined (5), where X = D denotes the diffusion process and X = E refers to the exponential correlation process that accounts for the volume fluctuations caused by the nuclear membrane undulations.

We next consider the situation in which the mCherry-labeled protein remains luminal, but the EGFP-tagged protein is membrane bound (denoted by the subscript ML). In this case, the exponential correlation term tsMSQ$_{\mathrm{gg,E}}$ of the green channel disappears because the fluorescence intensity of membrane-bound EGFP is unaffected by the nuclear membrane undulations. Consequently, the tsMSQ$_{\mathrm{gr}}$ curve for a pair of noninteracting proteins is given by

$$\mathrm{tsMSQ}^{(-)}_{\mathrm{gr,ML}}\left(T_{seg}\right) = f_{\mathrm{ct}}\mathrm{tsMSQ}_{gg,D}\left(T_{seg}\right), \tag{4}$$

which has a nonzero amplitude arising from the spectral cross talk of EGFP. For convenience, we subtract the spectral cross talk component and define the cross talk corrected cross-correlation function as

$$\mathrm{CC}\left(T_{\mathrm{seg}}\right) = \mathrm{tsMSQ}_{\mathrm{gr}}\left(T_{\mathrm{seg}}\right) - f_{ct}\mathrm{tsMSQ}_{\mathrm{gg}}\left(T_{\mathrm{seg}}\right), \tag{5}$$

which is calculated from the raw data using Eq. 2 and the definition of tsMSQ$_{\mathrm{gg}}$ given by Eq. 1. Applying Eq. 5 to Eqs. 3 and 4 yields

$$\mathrm{CC}_{\mathrm{LL}}\left(T_{\mathrm{seg}}\right) = \frac{F_{\mathrm{mCh}}}{F_g}\mathrm{tsMSQ}_{gg,E}\left(T_{\mathrm{seg}}\right) \tag{6}$$

and

$$\mathrm{CC}_{\mathrm{ML}}\left(T_{\mathrm{seg}}\right) = 0, \tag{7}$$

respectively, with $F_{\mathrm{mCh}} = F_r - f_{ct}F_g$ denoting the total fluorescence intensity of the mCherry-labeled proteins. Thus, membrane-associated EGFP-labeled proteins have a cross-correlation amplitude of 0 (Eq. 7), whereas luminal EGFP-labeled proteins have a positive cross-correlation amplitude (Eq. 6). This allows for the differentiation between luminal and membrane-associated EGFP-tagged proteins within the NE by comparing the measured CC value with the predictions based on Eqs. 6 and 7.

To ensure a sufficiently detectable difference between luminal and membrane-associated EGFP-tagged NE proteins, a segment time T_{seg} should be chosen that maximizes the value of the tsMSQ$_{\mathrm{gg,E}}$ function described in Eq. 6. Because the local NE volume fluctuations have a characteristic time of ~1 s, we chose a 6 s segment time T_0 to ensure that the value of tsMSQ$_{\mathrm{gg,E}}$ is close to its maximal amplitude A_0 (5). This amplitude is analytically determined by $A_0 = c^2\tau_s F_g$, where $c = \sqrt{\langle \Delta h^2 \rangle}/\langle h \rangle$ is the ratio of the root mean-square of the NE lumen height fluctuations/the average NE lumen height (4). For simplicity, we refer to the amplitude of the cross talk corrected cross-correlation function (Eq. 5) as $\Delta^{(\mathrm{CC})}$. Thus, the expected amplitudes of Eqs. 6 and 7 with a segment time of $T_0 = 6$ s are given by

$$\Delta^{(\mathrm{CC})}_{\mathrm{LL}} \approx c^2\tau_s F_{\mathrm{mCh}} \tag{8}$$

for luminal and

$$\Delta^{(\mathrm{CC})}_{\mathrm{ML}} = 0 \tag{9}$$

for membrane-bound NE proteins tagged with EGFP.

Finally, in the case that the EGFP-labeled NE protein exists as a mixture of luminal and membrane-associated states, we expect a cross-correlation amplitude reflective of this composition,

$$\Delta^{(\mathrm{CC})}_{\mathrm{mixture}} = f_{\mathrm{lumen}}\Delta^{(\mathrm{CC})}_{\mathrm{LL}} + (1 - f_{\mathrm{lumen}})\Delta^{(\mathrm{CC})}_{\mathrm{ML}} = f_{\mathrm{lumen}}c^2\tau_s F_{\mathrm{mCh}}, \tag{10}$$

where f_{lumen} is the intensity fraction of the population found in the NE lumen. We experimentally determine the cross talk corrected cross-correlation amplitude by evaluating Eq. 5 for a segment time of $T_0 = 6$ s,

$$\Delta^{(\mathrm{CC})} = \mathrm{tsMSQ}_{\mathrm{gr}}(T_0) - f_{ct}\mathrm{tsMSQ}_{\mathrm{gg}}(T_0) \tag{11}$$

Diffusion between two parallel walls

Consider a sphere of radius a with a diffusion coefficient D_{SE} given by the Stokes-Einstein relation that is placed into a narrow gap between two parallel walls. The diffusion coefficient D_p for parallel motion of the sphere with respect to the walls needs to account for wall-drag interactions, $D_p = \mu(d, a, z)D_{\mathrm{SE}}$, in which the correction factor μ depends on the fluid thickness d between the two walls, the radius a of the sphere, and the distance z of the sphere center from the nearest wall. This correction factor has been approximated by (27),

$$\mu(d, a, z) \approx 1 - \frac{9}{16}\left(\frac{a}{z} + \frac{a}{d - z}\right) \tag{12}$$

We assume that spheres are uniformly distributed, which allows us to average over the distance z of the sphere from the nearest wall, $\mu(d, a) = \int_a^{d-a}\mu(d, a, z)dz/(d - 2a)$, leading to the distance-averaged correction factor

$$\mu(d,a) \approx 1 + \frac{9}{8}\frac{a}{d-2a}\ln\frac{a}{d-a} \tag{13}$$

Because the diffusion coefficient and the diffusion time are inversely related, the corrected diffusion time of a sphere between two narrow walls is

$$\tau_p(n) = \frac{\tau_{SE}(n)}{\mu(d,a(n))}, \tag{14}$$

where τ_{SE} is the diffusion time based on the Stokes-Einstein relation. Equation 14 explicitly includes the dependence of the sphere radius and diffusion times on the degree of oligomerization n because the experimental test of the model is performed on concatenated fluorescent proteins as a function of n. Assuming spherical shape, the radius grows as $a(n) = a_1 n^{1/3}$, where a_1 represents the hydrodynamic radius of a single fluorescent protein. We choose a_1 of 2.3 nm, which represents the experimentally determined radius of gyration of EGFP (28). Because the Stokes-Einstein relation specifies a linear relation between the diffusion time and radius, we write $\tau_{SE}(n) = \tau_{SE,1} n^{1/3}$, with $\tau_{SE,1}$ representing the Stokes-Einstein diffusion time of a monomeric fluorescent protein.

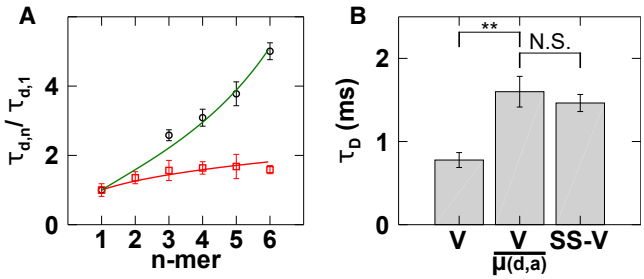

FIGURE 2 τ_D of Venus n-mers measured within the cytoplasm and NE. (*A*) Plot of τ_D vs. increasing number of covalently linked Venus proteins measured in the cytoplasm ($Venus_n$, *red squares*) or in the NE (SS-$Venus_n$, *black circles*) normalized to the τ_D of a Venus monomer within the respective environment is given. The cytoplasmic data follow the Stokes-Einstein relation, namely $\tau_D \propto \sqrt[3]{n}$ (*red line*), whereas the lumen data were fitted to Eq. 14 (*green line*). Error bars represent the standard error across $n \geq 5$ cells. (*B*) Plot of the mean τ_D for Venus monomer in the cytoplasm (V), the mean expected value for measurements of SS-Venus in the NE ($V/\mu(d,a)$), and mean measured value for SS-Venus in the NE (SS-V) is given. $^{**}p < 0.01$ as determined from a two-sided Welch's t-test. N.S., not significant ($p > 0.05$). To see this figure in color, go online.

RESULTS

To be able to develop new methods for distinguishing between soluble and membrane-associated NE proteins, we first needed to better understand the mobility of EGFP within the unique environment of the NE. Our recently published FFS results demonstrated that the mobility of EGFP within the NE lumen was reduced threefold relative to its mobility within the cytoplasm (4). To further explore this result, we investigated the dependence of the translational diffusion of EGFP within these two subcellular environments on its molecular weight (MW). To achieve this goal, we first performed FFS measurements within the cytoplasm of U2OS cells expressing the fluorescent protein Venus and its tandem oligomeric constructs ($Venus_n$ with n = 2–6) (17). The tsMSQ of each sample was then calculated and subsequently fitted to a single-species model to extract the diffusion time $\tau_{D,n}$ for each n-mer. The diffusion time increases weakly with the number of repeats, as expected from the Stokes-Einstein relation (Fig. 2 *A*), which is expected to hold for noninteracting globular proteins. The diffusion times were normalized to the diffusion time of the Venus monomer to facilitate comparison with the FFS results measured in the NE lumen described below.

To test the dependence of the translational diffusion of EGFP on molecular mass within the NE lumen, we performed FFS measurements within this subcellular environment in cells expressing SS-$Venus_n$ (n = 1, 3, 4, 5, 6). The presence of the SS of the luminal ATPase torsinA at the N-terminus of these constructs, which is cleaved off by the signal peptidase complex after protein synthesis, enables their targeting to the contiguous lumens of the ER and the NE (29). FFS data for these constructs were obtained at low intensities ($F_g < 60$ kHz) to effectively remove the impact of the previously identified nuclear membrane undulations on their analysis by tsMSQ (24). Thus, the resulting tsMSQ curves generated for these luminal SS-Venus constructs were fitted to a single-species model.

We found that the molecular-mass-dependent increase in $\tau_{D,n}$ for Venus expressed in the NE lumen was significantly more pronounced than what was observed for Venus expressed in the cytoplasm (Fig. 2 *A*), signaling a breakdown of the Stokes-Einstein relation. Because the NE lumen is a narrow liquid layer found between the INM and ONM (Fig. 1 *A*), proteins diffusing within the lumen will inherently be found in close proximity to membrane walls. This intimate proximity induces a hydrodynamic coupling of the fluid field surrounding the diffusing protein with the membrane wall, resulting in an increased drag experienced by the molecule.

The diffusive behavior of a protein found in close proximity to a single wall is well known (27). However, the presence of a second nearby wall results in additional hydrodynamic coupling interactions between the protein and the walls. Although these additional interactions have yet to be fully solved, an approximate solution does exist (27). We used this approximation after averaging across the distance between the protein and a given wall (Eq. 14) to describe our experimentally measured diffusion times and found a good agreement between the data and the resulting fit (Fig. 2 *A*), suggesting that additional drag from the nearby walls provides a reasonable model for explaining the strong dependence of protein mobility on MW in the NE lumen. The fit was performed with the experimentally determined value of 2.3 nm for the radius of gyration for a monomeric fluorescent protein (28), which leaves the distance d between the walls as the only free fit parameter. The recovered value of $d = 12$ nm indicates a spacing between the nuclear membranes that is significantly less than the

expected value of ~40 nm (1). This difference illustrates that modeling the INM and ONM as rigid walls is an oversimplification that will be discussed in more detail in the Discussion below. Therefore, the d we report serves as an effective width for modeling the mobility of the diffusing fluorescent protein within the NE lumen.

To further validate our model of protein diffusion within the NE lumen, we used Eq. 14 to predict the absolute diffusion time of EGFP in the NE lumen from our previously measured cytoplasmic diffusion time of Venus ($\tau_D = 0.88 \pm 0.09$ ms), which represents the Stokes-Einstein diffusion time. Inserting an effective width d of 12 nm into the model led to a good agreement between the expected ($\tau_D = 1.6 \pm 0.2$ ms) and measured ($\tau_D = 1.46 \pm 0.10$ ms) values for the luminal diffusion time of SS-Venus (Fig. 2 *B*). This result further supports our observation that the τ_D of proteins in the NE lumen is effectively described by modeling the two nuclear membranes as rigid walls with an effective width d. Collectively, these findings suggest that experimentally measured mobility cannot be reliably used to differentiate soluble from membrane-associated proteins within the NE.

A nontrivial complication for measuring protein mobility within the NE is the presence of nuclear membrane undulations that result in slow changes of the local NE volume over time (4). In addition to being slow, these undulations were shown to have a characteristic lateral scale at least as large as the lateral beam waist of our PSF (~0.45 μm), as discussed in more detail in Hennen et al. (4). Although these undulations have a negligible effect on the measured fluorescence signal of EGFP-tagged NE membrane proteins, they introduce a slow correlation process with an exponential decay on top of the fluorescence fluctuations generated by the EGFP-tagged luminal proteins or the fluorescence signal of EGFP-tagged NE membrane proteins (Fig. 1, *A–C*). This process can be identified by tsMSQ analysis, and it gives rise to an additional fluctuation amplitude A_0 (Fig. 1 *D*), with $A_0 = c^2\tau_s F$ being proportional to the average intensity F, with the average fractional height fluctuation c in the lumen represented by $c = \sqrt{\langle \Delta h^2 \rangle}/\langle h \rangle$ and the photon count sampling time being τ_s (4). This observation motivated further characterization of the membrane undulations to establish assays for differentiating between luminal and membrane-associated protein populations within the NE.

We hypothesized that the local NE volume fluctuations induced by nuclear membrane undulations are at least partially thermodynamically driven. Thus, lowering the temperature of the cells should result in a reduction of the amplitude A_0. If the process were strongly dependent on temperature, we might be able to diminish A_0 to negligible values by lowering the temperature by a few degrees. Such a reduction in A_0 would drastically simplify the analysis of FFS data collected within the NE. To investigate the feasibility of this approach, we measured A_0 in the NE of cells expressing different concentrations of SS-EGFP, as indicated by a range of F_g, at two distinct temperatures (35 and 10°C). As expected, we found that A_0 of SS-EGFP was proportional to its fluorescence intensity in cells measured at either temperature (Fig. 3 *A*). Although we observed a reduction in the slope of A_0 vs. F_g in cells measured at 10°C (Fig. 3 *A*), the nuclear membrane undulations still need to be accounted for, at least at higher-intensity values.

We further tested for nonthermal intracellular sources of the nuclear membrane undulations by performing additional experiments under two different conditions. First, ATP was depleted through the addition of azide and 2-deoxyglucose, which resulted in no significant change in the slope of A_0 vs. F_g (Fig. 3 *D*), indicating that the undulations are not actively driven. Second, we depolymerized microtubules with nocodazole, which caused a slight reduction in the slope of A_0 vs. F_g. However, this reduction was not statistically significant ($p = 0.06$) (Fig. 3 *D*), suggesting that microtubule-dependent processes are not a significant driver of the observed undulations.

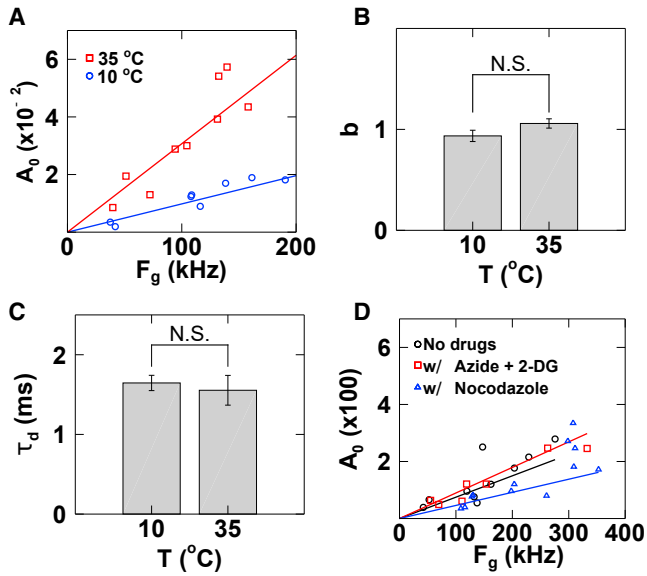

FIGURE 3 Results of FFS measurements of SS-EGFP performed in the NE at varied cell conditions. (*A*) Plot of A_0 vs. F_g of SS-EGFP measured in the NE of expressing cells at 35 (*red squares*) or 10°C (*blue circles*) with data fitted to a proportional function (*solid lines*) is given. (*B* and *C*) Plots of b vs. T (*B*) and τ_D vs. T (*C*) measured in the cells described in (*A*) are given. The mean b and τ_D and their standard errors were determined from multiple cell measurements ($n = 10$) for each construct. The b of SS-EGFP measured at 10 and 35°C was 0.94 ± 0.06 and 1.06 ± 0.05, respectively ($p = 0.6$). The τ_D of SS-EGFP measured at 10 and 35°C was 1.7 ± 0.1 and 1.6 ± 0.2 ms, respectively ($p = 0.9$). p-Values were determined by a two-sided Welch's t-test. N.S., not significant ($p > 0.05$). (*D*) Plot of A_0 vs. F_g of SS-EGFP measured at room temperature in the presence of no drugs (*black circles*), azide and 2-deoxyglucose (2-DG) (*red squares*), and nocodazole (*blue triangles*) is given. Fitted slopes are (7.5 ± 1.3) × 10^{-3}, (9.0 ± 1.1) × 10^{-3}, and (4.6 ± 0.5) × 10^{-3} kHz^{-1} for no drugs (*black line*), azide and 2-DG (*red line*), and nocodazole (*blue line*), respectively. To see this figure in color, go online.

In addition to A_0, tsMSQ analysis also recovers the brightness, b, and diffusion time, τ_D, of SS-EGFP in the NE of expressing cells (5,24). We previously showed that b and τ_D of SS-EGFP in the NE are both independent of fluorescence intensity (5). Here, we found that the value of b was 1 independent of temperature, consistent with SS-EGFP being a monomeric protein (Fig. 3 *B*). Surprisingly, we observed that the diffusion time of SS-EGFP within the NE was identical within experimental uncertainty in cells measured at either 35 or 10°C. This was surprising because the viscosity of water changes by a factor of ~2 between both temperatures (30).

To validate this unexpected result, we performed measurements on SS-EGFP in the NE of cells at 5°C increments over the range of 5–30°C. Again, we restricted our measurements to cells expressing low levels of SS-EGFP to minimize the impact of nuclear membrane undulations on the fluorescence fluctuation signals generated by the fluorescent protein (24). Our data demonstrate that SS-EGFP expressed in the NE exhibits a constant brightness (Fig. 4 *A*) and diffusion time (Fig. 4 *B*) over the entire temperature range. We also measured the previously described luminal proteins SS-EGFP-KASH2 (4), SS-Venus, and SS-Venus$_6$ in the NE of expressing cells at 5 or 35°C (Fig. S2). The results of these measurements revealed no statistically significant effect of temperature on τ_D of any of these fluorescently labeled proteins, suggesting that the independence of τ_D on temperature is a common feature of luminal NE proteins. Note that the temperature-independent mobility of both SS-Venus and SS-Venus$_6$ indicates that the size-dependent mobility curve (*green line*) in Fig. 2 *A* is not temperature dependent and therefore can be modeled by Eq. 14 using the same effective gap distance d. This observation implies that the NE thickness does not change with temperature.

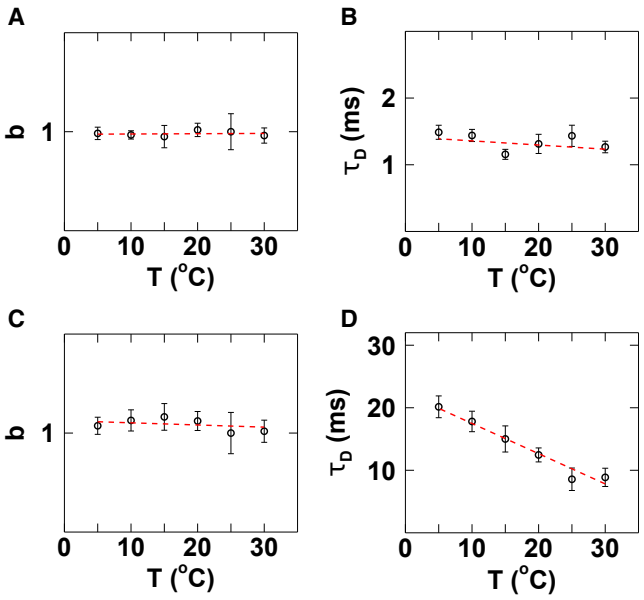

FIGURE 4 Temperature dependence of b and τ_D for a luminal and a membrane-bound NE protein. (*A* and *B*) Plots showing the average values and standard errors from measurements performed on $n = 6$ cells for b vs. T (*A*) and τ_D vs. T (*B*) for SS-EGFP are given. (*C* and *D*) Plots showing the average values and standard errors from measurements performed on $n = 6$ cells for b vs. T (*C*) and τ_D vs. T (*D*) for SS-EGFP- torsinA$^{NTD\text{-}2\times Leu}$ are given. Dashed line represents a linear fit of the data. All slopes are statistically indistinguishable from zero, except for (*D*) (slope = −0.48 ± 0.08 ms/°C). To see this figure in color, go online.

To determine whether this feature was shared by all NE proteins or was specific only for luminal NE proteins, we performed FFS measurements over the same temperature range in the NE of cells expressing the previously described membrane-associated SS-EGFP-torsinA$^{NTD\text{-}2\times Leu}$ (4,19). As observed with SS-EGFP, we found that b of SS-EGFP-torsinA$^{NTD\text{-}2\times Leu}$ was independent of temperature (Fig. 4 *C*). However, the diffusion time of this construct clearly decreased with increasing temperature (Fig. 4 *D*). This result agrees with our expectation of enhanced protein mobility in cells measured at higher temperatures as observed for proteins present in other model and live cell membranes (31).

For reference, we also measured the temperature dependence of b and τ_D for EGFP-tagged proteins in the cytoplasm and at the plasma membrane over the same temperature range. FFS data measured for EGFP in the cytoplasm and the previously described membrane-associated protein HRas-EGFP (21) at the plasma membrane reveal a temperature-independent b for both constructs at their respective subcellular locations (Fig. 5, *A* and *C*). Both EGFP and HRas-EGFP showed a statistically significant reduction in their τ_D with increasing temperature, with the slopes of their fit lines being −0.063 ± 0.015 and −0.61 ± 0.13 ms/°C, respectively (Fig. 5, *B* and *D*). Plotting the relative change in τ_D over the measured temperature range revealed similar behavior for EGFP, HRas-EGFP, and SS-EGFP-torsinA$^{NTD\text{-}2\times Leu}$ (Fig. S3). All three constructs closely followed the expected relative change in τ_D due to the temperature-dependent viscosity of water (30) (*dashed magenta line*, Fig. S3). This observed similarity was surprising and may be coincidental because previous work reported differences in the temperature-dependent scaling of mobility for different plasma membrane-associated proteins (31). Although we do not expect all proteins to follow this exact scaling of diffusion time with temperature, the trend of increasing τ_D with decreasing temperature appears to be common for membrane-bound proteins.

Taken together, our results indicate that the temperature independence of τ_D observed for luminal NE proteins over the experimentally measured range is an anomaly not shared by cytosolic, nuclear-membrane-associated, or plasma-membrane-associated proteins. Consequently, we may be able to harness this unique behavior of luminal NE proteins to experimentally distinguish them from membrane-associated NE proteins. We refer to this approach as the temperature-dependent mobility assay. Because a physical explanation for the temperature-independent τ_D of luminal

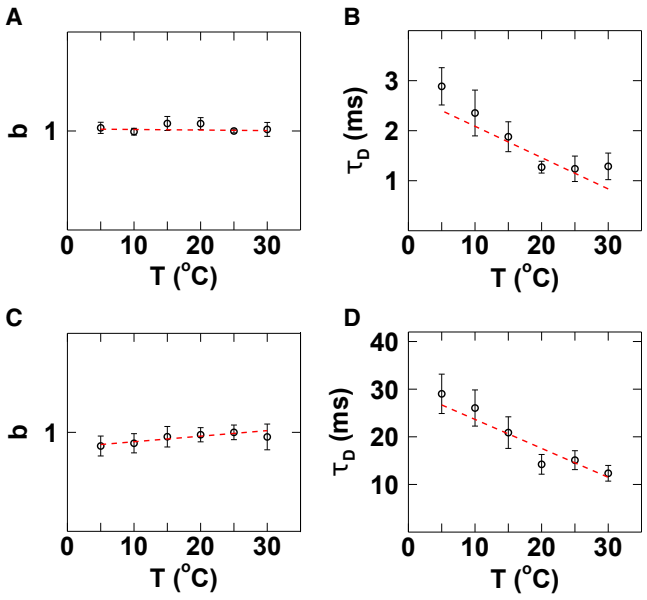

FIGURE 5 Temperature dependence of b and τ_D for plasma membrane-bound and cytoplasmic proteins. (*A* and *B*) Plots showing the average values and standard errors from measurements performed on $n = 6$ cells for b vs. T (*A*) and τ_D vs. T (*B*) for cytoplasmic EGFP are given. (*C* and *D*) Plots showing the average values and standard errors from measurements performed on $n = 8$ cells for b vs. T (*C*) and τ_D vs. T (*D*) for plasma membrane-bound HRas-EGFP are given. Dashed lines represent a linear fit to the data. To see this figure in color, go online.

NE proteins is currently lacking, we sought to identify a second differentiating marker between luminal and membrane-associated NE proteins to be able to independently verify the results obtained from the temperature dependence of the diffusional mobility assay described above.

Thus, we explored the potential of exploiting the presence of the nuclear-membrane-undulation-driven local NE volume changes as an orthogonal marker for distinguishing luminal from membrane-associated NE proteins (4). These local NE volume changes introduce an additional fluctuation component to the fluorescence signal generated by luminal NE proteins without affecting those generated by membrane-associated NE proteins (4,5). Although this difference has been used to distinguish both types of proteins (4,5), the method relies on a clear separation of the characteristic fluorescence fluctuation timescale between protein diffusion and NE volume undulations. For example, we have previously shown that a diffusion time of a few milliseconds and a volume fluctuation time of ~1 s are easily separable (5). However, it is particularly challenging to classify slowly diffusing proteins as luminal or membrane associated because the intensity fluctuations generated by their diffusion cannot be unequivocally discriminated from those generated by the local changes in the NE volume.

To overcome this challenge, we developed a new, to our knowledge, cross-correlation assay based on fluorescence cross correlation for distinguishing between membrane-bound and luminal NE proteins that is independent of their τ_D. This assay requires that FFS measurements be performed within the NE of cells that coexpress the protein of interest tagged with EGFP and the previously described luminal protein SS-mCherry-KDEL (20). For this assay to work, it is imperative that the EGFP-tagged protein of interest does not interact with SS-mCherry-KDEL.

We defined a cross-correlation amplitude $\Delta^{(CC)}$ between the green and red detection channels that is corrected for spectral cross talk. This amplitude is experimentally determined by tsMSQ analysis of the acquired FFS data (Eq. 11). In the absence of NE volume fluctuations, $\Delta^{(CC)}$ is zero for a pair of noninteracting EGFP- and mCherry-tagged NE proteins. However, if both proteins were noninteracting and luminal, they would experience identical NE volume fluctuations, resulting in the detection of coupled changes in the fluorescence intensities measured in the green and red detection channels (Fig. 6 *A*). This would produce a positive $\Delta^{(CC)}$-value in the absence of protein-protein interactions, with an amplitude that would be proportional to the mCherry fluorescence intensity (Eq. 8). If the EGFP-tagged protein were membrane associated, its fluorescence signal would be unaffected by the presence of local NE volume changes (Fig. 6 *B*). This would result in a fluorescence-intensity-independent $\Delta^{(CC)}$-value of zero (Eq. 9). By comparing the experimentally measured $\Delta^{(CC)}$ (Eq. 4) with the predicted behavior of Eqs. 7 and 8, $\Delta^{(CC)}$ provides an experimental marker for distinguishing between luminal and membrane-associated NE proteins.

To experimentally test whether $\Delta^{(CC)}$ provides a reliable marker for distinguishing luminal from membrane-associated NE proteins, we performed FFS measurements within the NE of cells coexpressing SS-mCherry-KDEL and SS-EGFP or SS-EGFP-torsinA$^{NTD\text{-}2\times Leu}$, which are the same EGFP-tagged model NE proteins used in the temperature-dependent mobility assay described above (Fig. 4). Importantly, SS-mCherry-KDEL was previously shown not to interact with either SS-EGFP or SS-EGFP-torsinA$^{NTD\text{-}2\times Leu}$ (20). As expected from Eq. 8, the $\Delta^{(CC)}$ of SS-mCherry-KDEL and SS-EGFP significantly increased in a proportional fashion (*dashed line*, slope $= 0.010 \pm 0.001$ kHz^{-1}) as a function of mCherry fluorescence intensity (Fig. 6 *C*, *black circles*). In contrast with this result, the $\Delta^{(CC)}$ of SS-mCherry-KDEL and SS-EGFP-torsinA$^{NTD\text{-}2\times Leu}$ was independent of the fluorescence intensity of mCherry, with an amplitude of ~0 (Fig. 6 *C*, *red squares*). Because this result agrees with our predictions from Eq. 9, these proof-of-principle experiments demonstrate that the corrected $\Delta^{(CC)}$ between an EGFP-tagged NE protein of interest and SS-mCherry-KDEL provides a second, independent assay for determining whether a NE protein is luminal or membrane associated. We refer to this method as the luminal cross-correlation assay.

Until now, we have only used the above-described temperature-dependent mobility and luminal cross-correlation assays to study model fluorescently labeled NE proteins that are either purely luminal or membrane associated.

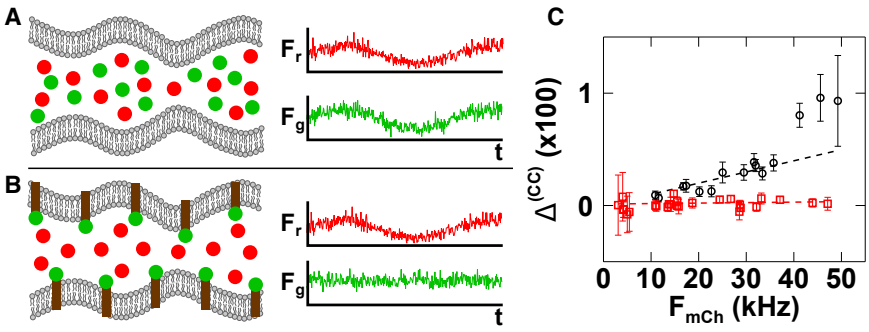

FIGURE 6 Cross-correlation amplitude $\Delta^{(CC)}$ between a noninteracting mCherry- and EGFP-tagged protein in the presence of membrane undulations. (*A*) The illustration on the left shows that a pair of noninteracting luminal mCherry- or EGFP-tagged NE proteins experience identical nuclear-membrane-undulation-driven changes in local NE volume, resulting in the detection of concomitant fluorescence intensity fluctuations in the green and red channels. These concomitant fluctuations, which are conceptually depicted as a sinusoidal modulation of the fluorescence signal over time in the illustrative plot shown to the right, give rise to a positive $\Delta^{(CC)}$. (*B*) The illustration on the left shows an mCherry-tagged luminal NE protein that does not interact with a membrane-associated EGFP-tagged NE protein. Because only the intensity fluctuations generated by the luminal mCherry-tagged NE protein are affected by the presence of nuclear-membrane-undulation-driven local changes in NE volume, the value of the $\Delta^{(CC)}$ for this pair of proteins is ~0. (*C*) Plot of $\Delta^{(CC)}$ and standard deviations vs. mCherry intensity from FFS measurements performed in the NE of cells coexpressing SS-mCherry-KDEL and SS-EGFP (*black circles*, $n = 15$) or SS-EGFP-torsinA$^{NTD\text{-}2\times Leu}$ (*red squares*, $n = 26$) with fitted slopes of 0.010 ± 0.001 kHz^{-1} (*black dashed line*) and 0.0009 ± 0.0006 kHz^{-1} (*red dashed line*), respectively, is given. To see this figure in color, go online.

However, it is reasonable to assume that physiologically relevant NE proteins may exist as a mixture of these two states. Although we have developed a theory (Eq. 10), which is tested later in this section, for how the luminal cross-correlation assay would behave under this condition, we wanted to determine if the temperature-dependent mobility assay was capable of identifying such mixtures. To begin to achieve this goal, we used the temperature-dependent mobility assay to perform measurements in the NE of cells that coexpress SS-EGFP-torsinA$^{NTD\text{-}2\times Leu}$ and SS-mCherry-KDEL at different temperatures. These measurements were specifically performed at 1010 nm to ensure identical Q-values for both EGFP and mCherry. Because the luminal SS-mCherry-KDEL and the membrane-associated SS-EGFP-torsinA$^{NTD\text{-}2\times Leu}$ are distinguishable by their fluorescence emission colors, we analyzed the tsMSQ curve of the red and green detection channels independently as described in the Material and Methods. Specifically, data obtained from the red channel were fitted to a two-species model with a fast-diffusing species associated with SS-mCherry-KDEL and a slow-diffusing species caused by the cross talk from SS-EGFP-torsinA$^{NTD\text{-}2\times Leu}$. Because cross talk from mCherry is negligible, the data obtained from the green channel were fitted to a single-species model. The result of these analyses revealed that the temperature dependence of the fitted τ_D agrees with our expectations. Specifically, the τ_D for SS-mCherry-KDEL measured in the red channel was temperature independent (slope = −0.001 ± 0.004 ms/°C) (Fig. 7 *A*), as expected for a luminal NE protein. However, the τ_D for SS-EGFP-torsinA$^{NTD\text{-}2\times Leu}$ measured in the green channel exhibited a significant decrease with increasing temperature (slope = −2.1 ± 0.2 ms/°C) (Fig. 7 *B*), as expected.

Next, we combined the photon count records measured in the red and green channels to create a data set that represents a binary mixture of a luminal and membrane-associated NE proteins. The tsMSQ curve of this new data set was then fitted to a two-species model to recover the two distinct diffusion times of the mixture. Although the τ_D of the fast-diffusing species showed no significant dependence on temperature (slope = 0.011 ± 0.006 ms/°C) (Fig. 7 *C*), the τ_D of the slow-diffusing species decreased strongly with increasing temperature (slope = −2.1 ± 0.3 ms/°C) (Fig. 7 *D*). These results agree with the individual analysis of the data generated from the red and green channels (Fig. 7, *A* and *B*) and demonstrate that the temperature-dependent mobility assay can accurately differentiate luminal from membrane-associated species in a binary mixture of NE proteins with distinct diffusion times.

In addition to τ_D, we recovered amplitudes a_{fast} and a_{slow} (representing SS-mCherry-KDEL and SS-EGFP-torsinA$^{NTD\text{-}2\times Leu}$, respectively) for each diffusing species (Fig. S4, *A* and *B*). These amplitudes are related to the intensity fraction by $a_i = f_i Q_i$, with f_i and Q_i denoting the intensity fraction and Q-value of species i, respectively (4). Because the Q-values of SS-mCherry-KDEL (Q_{fast}) and SS-EGFP-torsinA$^{NTD\text{-}2\times Leu}$ (Q_{slow}) are identical in this experiment, the luminal fraction f_{lumen} is given by $f_{lumen} = a_{fast}/(a_{fast} + a_{slow})$. The analysis revealed that f_{lumen} is independent of temperature (slope = 0.002 ± 0.002°C^{-1}) with a mean and standard error of f_{lumen} = 0.40 ± 0.03 (Fig. S4 *C*). To provide an independent check, we directly calculated the intensity fraction f_{lumen} using the photon count records from both channels, resulting in a mean and standard error of 0.33 ± 0.03, which is in good agreement with the amplitude-derived fraction.

We then turned our attention to the SS-EGFP-tagged luminal domain of SUN2 construct, SS-EGFP-SUN2$^{261–731}$, which we previously characterized by FFS (4–6). The results of these studies suggested a model in which SS-EGFP-SUN2$^{261–731}$ transitions from being a fast-diffusing monomer to a slow-diffusing homotrimer as a function of its concentration. We had hypothesized that the fast-diffusing monomer of SS-EGFP-SUN2$^{261–731}$ was luminal, whereas the slow-diffusing homotrimer of this protein was membrane associated. However, we lacked experimental evidence to confirm

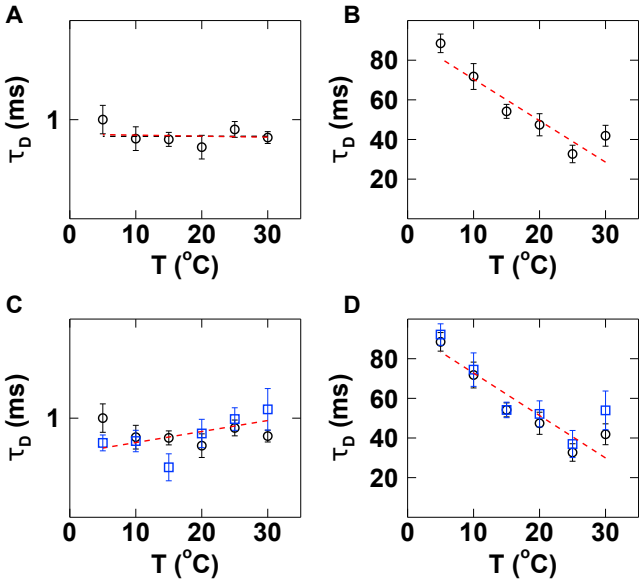

FIGURE 7 τ_D vs. T averages and standard errors from FFS measurements performed in $n = 8$ cells coexpressing SS-EGFP-torsinA$^{NTD\text{-}2\times Leu}$ and SS-mCherry-KDEL. (*A*) Plot of τ_D vs. T of the red detection channel characterizes SS-mCherry-KDEL. (*B*) Plot of τ_D vs. T of the green detection channel characterizes SS-EGFP-torsinA$^{NTD\text{-}2\times Leu}$. (*C*) Plot of the fast τ_D component from two-species analysis of the combined data from the red and green channel (*blue squares*) and results from (*A*) (*black circles*) vs. T are shown. (*D*) Plot of the slow τ_D component from two-species analysis of the combined data from the red and green channel (*blue squares*) and results from (*B*) (*black circles*) vs. T are shown. Dashed lines represent a linear fit to the data. To see this figure in color, go online.

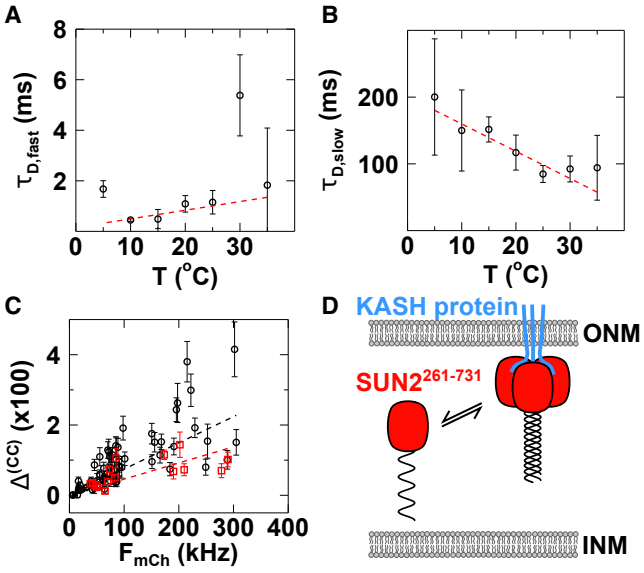

FIGURE 8 Temperature-dependent mobility and luminal cross-correlation assays performed on SS-EGFP-SUN2$^{261–731}$. (*A*) Plot of averages and standard errors of the fast τ_D component vs. T from FFS measurements performed in $n = 8$ cells expressing SS-EGFP-SUN2$^{261–731}$ with a linear fit of the data (*dashed red line*) is given. (*B*) Plot of averages and standard errors of the slow τ_D component vs. T from FFS measurements performed in $n = 8$ cells expressing SS-EGFP-SUN2$^{261–731}$ with a linear fit of the data (*dashed red line*) is given. (*C*) Plot of $\Delta^{(CC)}$ and standard deviations vs. F_{mCh} from measurements performed within the NE of cells coexpressing SS-EGFP-SUN2$^{261–731}$ and SS-mCherry-KDEL is given. Data were collected in cells expressing low ($F_g < 60$ kHz, *black circles*, $n = 64$) or high ($F_g \geq 60$ kHz, *red squares*, $n = 16$) levels of SS-EGFP-SUN2$^{261–731}$ and subsequently fitted to a proportional function as represented by the dashed black and red lines, respectively. (*D*) An illustrative model of SS-EGFP-SUN2$^{261–731}$ (*red*) assembly with luminal monomers that transition into homotrimers associated with the ONM through interactions with endogenous KASH proteins (*blue*) is shown. To see this figure in color, go online.

or refute this hypothesis because as luminal proteins form larger complexes, their mobility is expected to reduce significantly (Fig. 2 *A*). Armed with the temperature-dependent mobility and the luminal cross-correlation assays, we now sought to test our hypothesis.

We first used the temperature-dependent mobility assay. To do this, we performed FFS measurements in the NE of cells expressing of SS-EGFP-SUN2$^{261–731}$ over a range of temperatures. We identified the fast- and slow-diffusing components from these data by fitting the tsMSQ function to a two-species diffusion model (4,5). As expected for a luminal NE protein, we did not observe a significant dependence of τ_D on temperature (slope $= 0.03 \pm 0.04$ ms/°C) for the fast-diffusing species of SS-EGFP-SUN2$^{261–731}$ (Fig. 8 *A*). In contrast, the slow-diffusing SS-EGFP-SUN2$^{261–731}$ species did exhibit a significant decrease in τ_D with increasing temperature (slope $= -4.1 \pm 1.0$ ms/°C) (Fig. 8 *B*). These results provide experimental evidence that supports our hypothesis that the fast-diffusing species of SS-EGFP-SUN2$^{261–731}$ is luminal, whereas the slow-diffusing species is membrane associated. As before, we recovered the amplitudes a_{fast} and a_{slow} in addition to the diffusion times. The relationship between Q_{fast} and Q_{slow} has been previously established as $Q_{fast} = 1/3Q_{slow}$ (4), resulting in $f_{lumen} = a_{fast}/(a_{fast} + 1/3a_{slow})$. Applying this relation, we obtained f_{lumen} as a function of temperature (Fig. S5). Although a fit to a linear function identified a slight increase of f_{lumen} with temperature, the slope is statistically indistinguishable from zero (slope $= 0.005 \pm 0.002$°C^{-1}). We recovered a mean and standard error of $f_{lumen} = 0.42 \pm 0.03$ (Fig. S5).

We further applied the luminal cross-correlation method to this protein system to check whether both assays lead to the same conclusion. Because we expect a positive slope of the amplitude $\Delta^{(CC)}$ vs. F_{mch} for luminal proteins and a slope and amplitude of zero for membrane-associated proteins, a binary mixture of these two protein species should be reflected in the measured slope, assuming no change in the ratio between the average membrane undulation amplitude/lumen thickness. FFS measurements performed in the NE of cells coexpressing SS-EGFP-SUN2$^{261–731}$ and SS-mCherry-KDEL revealed a significant increase in $\Delta^{(CC)}$ with increasing mCherry fluorescence intensity F_{mCh}. This result indicates the presence of a luminal protein component (Fig. 8 *C*). We find that the slopes of the $\Delta^{(CC)}$ determined from measurements performed in cells expressing high ($F_g \geq 60$ kHz,

slope = 0.0075 ± 0.0005 kHz^{-1}) and low (F_g < 60 kHz, slope = 0.0046 ± 0.0006 kHz^{-1}) concentrations of SS-EGFP-SUN2$^{261–731}$ are significantly different from each other. Given the previously reported monomer/trimer equilibrium of SS-EGFP-SUN2$^{261–731}$ (6,24), the fraction of luminal SS-EGFP-SUN2$^{261–731}$ monomers is higher at low protein concentrations than at higher protein concentrations. Analyzing these slopes with Eq. 10 results in an average f_{lumen} value of 0.35 ± 0.05 and 0.23 ± 0.09 at low and high SS-EGFP-SUN2$^{261–731}$ concentrations, respectively. Note that the value of f_{lumen} at low concentration (0.35 ± 0.05) nicely agrees with the independently determined f_{lumen} (0.42 ± 0.03) found by the temperature-dependent mobility assay that was performed at low concentrations. To confirm that the expression of SS-EGFP-SUN2$^{261–731}$ does not affect the relative membrane undulation amplitudes, thereby altering c in Eq. 10, we compared the slope of A_0 vs. F in the presence and absence of SS-EGFP-SUN2$^{261–731}$ and observed no significant difference (Fig. S6).

To further validate the luminal cross-correlation assay of SS-EGFP-SUN2$^{261–731}$, we independently calculated f_{lumen} from the fitted amplitudes using $f_{lumen} = a_{fast}/(a_{fast} + 1/3a_{slow})$. This analysis resulted in f_{lumen} = 0.40 ± 0.10 for the low-expressing cells and f_{lumen} = 0.33 ± 0.05 for high-expressing cells, in agreement with the luminal cross-correlation assay. Furthermore, we independently determined the fraction of SS-EGFP-SUN2$^{261–731}$ monomers within the monomer/trimer equilibrium from the brightness of the data collected by the green channel as previously described (4). This resulted in average $f_{monomer}$ values of 0.34 ± 0.02 and 0.21 ± 0.03 for the low and high SS-EGFP-SUN2$^{261–731}$ concentration data, respectively. Thus, we conclude that the SS-EGFP-SUN2$^{261–731}$ monomer is luminal and the SS-EGFP-SUN2$^{261–731}$ homotrimer is membrane associated. The observed reduction in slope at higher protein concentrations is consistent with a decrease in the fraction of the luminal monomer species as SS-EGFP-SUN2$^{261–731}$ transitions to a membrane-associated homotrimer. This finding provides further support for a model of SS-EGFP-SUN2$^{261–731}$ assembly in which fast-diffusing luminal monomers transition into slowly diffusing membrane-associated homotrimers (Fig. 8 *D*).

Finally, we used the methods described above to investigate the influence of tagging the N-terminus or C-terminus of the luminal AAA+ protein torsinA on its ability to associate with nuclear membranes. TorsinA functions within the NE to promote the assembly of functional LINC complexes as well as the interphase assembly of nuclear pore complexes (16). The hydrophobic N-terminal domain (NTD) of torsinA enables its monotopic membrane association and retention within the ER and NE (19).

Our previous studies showed that a WT torsinA construct containing EGFP inserted immediately after the ER/NE lumen-targeting N-terminal SS (SS-EGFP-torsinA^{WT}) was able to rescue the ability of torsinA-null fibroblasts to properly orient their centrosomes, which is a LINC-complex-dependent process (16). Given the close proximity of EGFP to the NTD, it is possible that the ability of SS-EGFP-torsinA^{WT} to associate with the nuclear membranes will be compromised. Consistent with this possibility, SS-EGFP-torsinA^{WT} showed no τ_D dependence on temperature, with a slope of −0.15 ± 0.13 ms/°C (Fig. 9 *A*). To further test the hypothesis that tagging the N-terminus of torsinA negatively impacts its membrane association, we performed the temperature-dependent mobility assay in cells expressing a previously described construct in which EGFP is fused to the C-terminus of torsinA (SS-torsinA^{WT}-EGFP) (32). We found that SS-torsinA^{WT}-EGFP exhibited a strong decrease in τ_D with increasing temperature (slope = −5.7 ± 1.7 ms/°C), consistent with it being a membrane-associated protein (Fig. 9 *B*).

We then expressed either SS-EGFP-torsinA^{WT} or SS-torsinA^{WT}-EGFP with SS-mCherry-KDEL to perform cross-correlation experiments. The cross-correlation amplitude $\Delta^{(CC)}$ of SS-torsinA^{WT}-EGFP increased with the intensity of SS-mCherry-KDEL measured in the red channel (slope = 0.0027 ± 0.0005 kHz^{-1}), whereas $\Delta^{(CC)}$ of

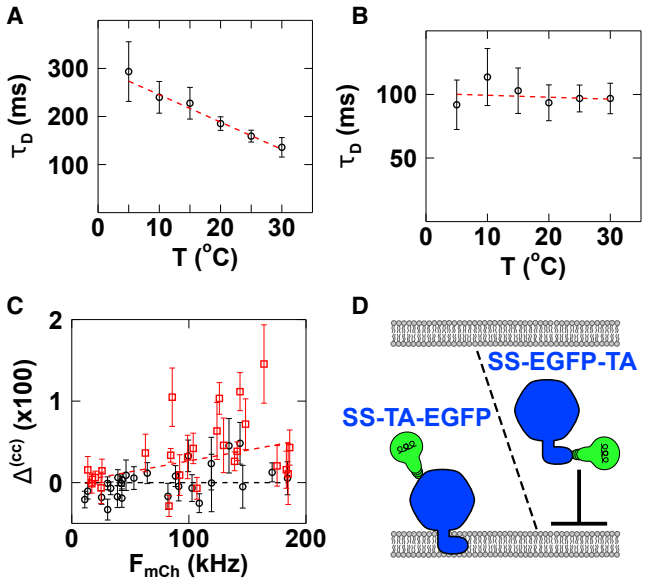

FIGURE 9 FFS analysis of torsinA constructs. (*A*) Plot of averages and standard errors of τ_D vs. T from FFS measurements performed on n = 8 cells expressing SS-torsinA-EGFP (C-terminal tagged) with a fit to a linear function (*red dashed line*) is shown. (*B*) Plot of averages and standard errors of τ_D vs. T from FFS measurements performed on n = 10 cells expressing SS-EGFP-torsinA (N-terminal tagged) with a fit to a linear function (*red dashed line*) is given. (*C*) Cross-correlation amplitude $\Delta^{(CC)}$ and standard deviations vs. fluorescence intensity F_{mCh} of SS-mCherry-KDEL in the presence of SS-torsinA^{WT}-EGFP (*black circles*, n = 27) and SS-EGFP-torsinA^{WT} (*red squares*, n = 26) with fitted slopes (*black* and *red dashed lines*, respectively) is shown. (*D*) An illustrative model of torsinA (TA) (*blue*) tagged with EGFP (*green light bulb*) is shown. C-terminal-tagged torsinA (SS-TA-EGFP) associates with the membrane, whereas N-terminal-tagged torsinA (SS-EGFP-TA) lacks significant association with the membrane. To see this figure in color, go online.

SS-EGFP-torsinA^{WT} stayed near zero, independent of the intensity F_{mCh} of SS-mCherry-KDEL (slope = 0.0000 ± 0.0004 kHz^{-1}) (Fig. 9 *C*). These results are consistent with the above-described temperature-dependent mobility experiments (Fig. 9, *A* and *B*) and suggest a model in which the fusion of EGFP to the N-terminus of torsinA inhibits its membrane association, whereas fusing EGFP to the C-terminus of torsinA does not (Fig. 9 *D*).

DISCUSSION

Although fluorescence recovery after photobleaching and FFS techniques have been used to distinguish mobile and immobile populations of select NE proteins (33,34), the diffusive mobility of NE proteins remains a largely unexplored topic. Our study provides a first, to our knowledge, endeavor to systematically assess the mobility of luminal NE proteins. Importantly, we found a violation of the Stokes-Einstein relation for luminal NE proteins that we explain by their exposure to additional drag forces generated by near-wall effects. Surprisingly, a simple theory based on two rigid walls separated by a thin gap exhibited a good quantitative agreement with the experimentally measured diffusion time for luminal NE proteins as a function of their MW (Fig. 2 *A*). The only adjustable parameter of the fit model was the gap distance, which was estimated to be 12 nm. Thus, the gap distance is significantly smaller than the estimated ∼40 nm thickness of the NE (1). However, the NE is not bounded by two rigid walls but by two nonrigid nuclear membranes. In addition, the presence of proteins within the nuclear membrane and within the NE lumen increases the complexity of the system, which is currently beyond the reach of our model. The complexity of the model is further increased by the presence of nuclear membrane undulations that result in fluctuations in the gap distance. These complications likely have an effect on the free fit parameter of our model. Thus, we consider the fitted gap distance as an effective parameter for modeling NE protein diffusivity assuming rigid walls.

An important prediction of our model is the pronounced dependence of luminal NE protein diffusion time on MW, which we observed experimentally (Fig. 2 *A*). The upward curvature of the measured FFS data and the model reflect the nonlinear growth of Eq. 14 with particle radius a. Consequently, it is not practical to rely on diffusion for distinguishing between luminal and membrane-associated NE proteins. For example, the transmembrane protein SS-EGFP-torsinA$^{NTD\text{-}2\times Leu}$ has a diffusion time of ∼10 ms at room temperature (Fig. 4 *D*), whereas a luminal sixfold fluorescent protein concatemer has a diffusion time of ∼7 ms (Fig. S2 *C*). The approximate similarity of these values demonstrates the futility of using NE protein mobility as a diagnostic marker for membrane association. In contrast, soluble cytoplasmic proteins are typically more mobile than plasma-membrane-associated proteins because of the weak dependence of the diffusion coefficient on MW, consistent with the Stokes-Einstein relationship.

In an effort to devise a method that could distinguish between luminal and membrane-associated NE proteins in living cells, we asked whether we could take advantage of the previously reported selective sensitivity of luminal NE proteins to the presence of nuclear membrane undulations (4). The fluctuations observed by FFS arise from out-of-phase undulations of the two nuclear membranes, effectively changing the local volume of the lumen (4), the cause of which has not been extensively explored. To better understand the nature of these nuclear membrane undulations, we tested the hypothesis that they are thermally driven. Here, we provide clear evidence for a thermal contribution to these nuclear membrane undulations by observing a reduction in their fluctuation amplitude with increasing temperature (Fig. 3 *A*), whereas neither ATP depletion nor microtubule depolymerization significantly changed the fluctuation amplitude (Fig. 3 *D*). Surprisingly, we also found that the diffusion time of luminal NE proteins was temperature independent, unlike the diffusion time of membrane-associated NE proteins. It is important to note that one must be cautious when performing measurements at the low end of the temperature range shown here because temperature may affect the stability of protein complexes as well as cellular interactions and processes. Generally, the time cells spend at low temperatures should be minimized. We exploited this unusual and currently unexplained phenomenon to distinguish luminal and membrane-bound NE proteins in a method we refer to as the temperature-dependent mobility assay.

Although the temperature independence of luminal NE protein diffusion time is currently not understood, we speculate that it is related to the presence of nuclear membrane undulations. Let us first consider an NE with rigid nuclear membranes that are separated by the gap distance d_0 with a diffusion time τ_0 for a given luminal protein. We then allow fluctuations of the nuclear membranes around the average gap distance of d_0, which lead to time periods with a gap distance d in excess of d_0 and conversely to time periods with d less than d_0. Because of the presence of near-wall effects, NE protein diffusion time is slowed down with respect to τ_0 when the gap narrows by Δd and decreased when the gap widens by Δd. Because the near-wall effects on NE protein diffusion are nonlinear with respect to gap height (Eq. 13), the increase in diffusion time with respect to τ_0 for a narrowing of the gap by Δd is more pronounced than the reduction in diffusion time for a gap increase by Δd. Thus, we expect that the diffusion time observed in the presence of gap distance fluctuations would be increased relative to the diffusion time of proteins observed in the absence of nuclear membrane undulations. Furthermore, the nonlinear nature of Eq. 13 predicts that a larger fluctuation amplitude Δd in gap size results in a larger increase in protein diffusion time.

Our results (Fig. 6 *C*) show that a reduction in temperature results in a reduction in the fluctuation amplitude of the nuclear membrane undulations, which is consistent with a thermally activated process. The reduction in the gap distance fluctuations observed with decreased temperature is expected to decrease NE protein diffusion time as discussed above. However, reducing the temperature also increases the viscosity of the NE lumen, which increases NE protein diffusion time. Thus, the temperature-dependent effects of gap size fluctuations and viscosity on NE protein diffusion time oppose each other. We hypothesize that this opposition could potentially explain the apparent independence of τ_D on temperature observed for luminal NE proteins (Fig. 4 *B*), if the effects of temperature on gap size fluctuations and viscosity are compensatory. This hypothesis could be tested by experimentally varying the gap distance of the NE by simultaneously depleting SUN2 and the related SUN protein SUN1 by RNA interference or overexpressing the SUN1 luminal domain. Electron microscopy revealed that either treatment results in the expansion of the perinuclear space (2). It will be interesting to pursue this line of inquiry in the future.

Because the theoretical underpinnings of the temperature-dependent mobility assay are incompletely understood, we needed to develop a second test for independently validating the results obtained by this assay. We refer to our second test as the luminal cross-correlation assay because it differentiates luminal from membrane-associated NE proteins using a dual-color approach that takes advantage of the presence of nuclear membrane undulations (Fig. 6). The results we obtained studying model NE proteins with the temperature-dependent mobility assay closely agreed with those obtained studying the same proteins with the luminal cross-correlation assay. This agreement demonstrates the utility of both assays for distinguishing between luminal and membrane-associated proteins in the NE of living cells.

Nevertheless, it is important to note that each assay has its unique advantages and disadvantages. The most immediate difference between these assays is their instrumentation requirements. Whereas the luminal cross-correlation assay requires a dual-channel detection setup, the temperature-dependent mobility assay demands access to a temperature-controlled microscope stage. We found that a temperature range of at least 20°C should be explored to reliably establish a temperature-independent mobility (Figs. 4 and S2). If the maximal temperature of live cells is limited to 37°C, the stage needs to be able to cool below room temperature to explore a temperature differential of 20°C. For convenience, we restricted the use of the temperature-dependent mobility assay to cells expressing low protein concentrations (24). Performing the assay at higher protein concentrations complicates the data analysis because of the fact that the effect of nuclear membrane undulations on the fluorescence signal must be accounted for. In contrast, the analysis of the luminal cross-correlation assay is very simple (Eq. 11) and independent of the concentration of the expressed EGFP-tagged NE protein. However, the presence of a sufficiently high concentration of an mCherry-labeled reference NE protein is critical for the luminal cross-correlation assay because the signal amplitude is directly proportional to its fluorescence (Eq. 11).

Given that the temperature-dependent mobility and the luminal cross-correlation assays can readily differentiate between purely membrane-associated and purely luminal NE protein populations (Figs. 4 and 6), we next asked whether these assays could be used to study a binary mixture of these two protein populations. Our results indicate that the diffusion time of the luminal and membrane-associated species is an important consideration when using these two assays. In particular, if the diffusion times of the two protein populations differ sufficiently to be resolvable by tsMSQ, then the temperature-dependent mobility assay can accurately identify each NE protein species as luminal or membrane associated (Fig. 7). The fit amplitudes obtained from tsMSQ analysis provide further mechanistic insights into NE protein oligomerization, as previously described (4). However, if the diffusion times of the luminal and membrane-bound species were too close to be resolved, a single effective diffusion time would be recovered. Although the temperature dependence of this diffusion time should reflect the relative proportion of each species, we have little confidence in the quantitative nature of this approach because of the absence of a theoretical understanding of the underlying temperature-dependent mobility of each species.

The luminal cross-correlation assay is completely independent of diffusion time. Thus, even if the diffusion times were significantly different between a luminal and membrane-associated species, the luminal cross-correlation assay could not directly separate a mixture of these species because the assay relies solely on the tsMSQ amplitude. However, the composition of the mixture is reflected by the slope of the cross-correlation amplitude $\Delta^{(CC)}$ as a function of the mCherry fluorescence intensity according to Eq. 10. We demonstrated the soundness of this approach through measurements of the SUN2 luminal domain. Using Eq. 10, we determined the average luminal population fraction of SS-EGFP-SUN2$^{261–731}$ in cells expressing high or low levels of this construct. Both values were in good agreement with the average monomer fraction determined independently by brightness analysis, which identifies the monomer population as luminal and the homotrimer population as membrane associated. Although the diffusion times of the two SS-EGFP-SUN2$^{261–731}$ populations were resolvable in this experiment, we want to stress that the luminal cross-correlation assay provides an effective means to distinguish membrane-associated and luminal populations if their mobility is similar or identical. Thus, the two assays developed here are complementary. Although each assay may be performed on its own, we believe they are best used in conjunction with each other to combine their individual strengths.

The results of our SS-EGFP-SUN2$^{261–731}$ experiments support a previously proposed model for the homo-oligomerization of this construct, in which luminal monomers transition to membrane-associated homotrimers with increasing protein concentration (5). This model was originally based on the significant difference in diffusion times between the monomeric and trimeric species (4). However, the results of Fig. 2 demonstrate that large luminal complexes may exhibit significantly reduced mobility, thus requiring the application of the assays developed in this manuscript, which confirmed the hypothesized model. Because the homotrimerization of the SUN2 luminal domain is critical for KASH protein-binding (7), we interpret the observed membrane association of the SS-EGFP-SUN2$^{261–731}$ homotrimers as reflecting their association with endogenous KASH proteins present in the ONM. Because the transluminal interaction of SUN and KASH proteins forms the core of a LINC complex, future experiments designed to study the SUN-KASH interaction within its native subcellular environment will significantly increase our mechanistic understanding of LINC complex assembly, as well as the pathological impact of human-disease-associated genetic mutations in SUN proteins on nuclear-cytoskeletal coupling.

Fluorescent tags have the potential to significantly alter the function and properties of proteins (35,36). We identified a significant difference in the behavior of torsinA depending on whether EGFP was tagged to its N- or C-terminus. In particular, C-terminus-tagged torsinA associated with the nuclear membranes, whereas the N-terminus tagged construct is predominantly luminal. Although we cannot rule out transient membrane interactions or low populations of membrane-associated torsinA for the N-terminus-tagged construct, our results demonstrate a clear difference in the behavior of this construct and the C-terminus-tagged one. This finding is significant because torsinA constructs encoding EGFP fused to the N- or C-terminus of torsinA have been used in previous studies of the function of this AAA+ protein without much consideration of the potential impact of EGFP position (16,37,38). Thus, our assays have considerable potential for identifying labeling effects for NE protein with respect to their influence on membrane association. Although future work may improve and expand these assays, the results presented here clearly demonstrate their utility as a means for differentiating luminal and membrane-associated protein populations within the NE. For example, this knowledge may significantly advance our mechanistic understanding of torsinA-mediated processes, including the regulated assembly of functional LINC complexes as well as the interphase assembly of nuclear pore complexes.

SUPPORTING MATERIAL

Supporting Material can be found online at https://doi.org/10.1016/j.bpj.2020.03.025.

AUTHOR CONTRIBUTIONS

J.H., J.K., G.W.G.L., and J.D.M. were responsible for experimental design. J.H. and J.K. performed experiments. J.H., J.K., and J.D.M. performed analysis. C.A.S. and G.W.G.L. contributed reagents. S.R.K. developed experimental methods. J.H., G.W.G.L., and J.D.M. wrote the manuscript.

ACKNOWLEDGMENTS

We thank Steven Vogel (National Institutes of Health) for providing plasmids for the Venus concatamers and Phyllis Hanson (University of Michigan) for the SS-torsinA^{WT}-EGFP construct. We also thank Yan Chen (University of Minnesota) and Patrick T. Willey (University of Minnesota) for providing technical assistance.

This work was supported by the National Institutes of Health GM064589 (J.D.M., J.H., J.K., and S.R.K.) and GM129374 (G.W.G.L. and J.D.M.).

REFERENCES

1. Watson, M. L. 1955. The nuclear envelope; its structure and relation to cytoplasmic membranes. *J. Biophys. Biochem. Cytol.* 1:257–270.
2. Crisp, M., Q. Liu, …, D. Hodzic. 2006. Coupling of the nucleus and cytoplasm: role of the LINC complex. *J. Cell Biol.* 172:41–53.
3. Worman, H. J., and G. Bonne. 2007. "Laminopathies": a wide spectrum of human diseases. *Exp. Cell Res.* 313:2121–2133.
4. Hennen, J., K.-H. Hur, …, J. D. Mueller. 2017. Quantitative brightness analysis of protein oligomerization in the nuclear envelope. *Biophys. J.* 113:138–147.
5. Hennen, J., K.-H. Hur, …, J. D. Mueller. 2019. Protein oligomerization and mobility within the nuclear envelope evaluated by the time-shifted mean-segmented Q factor. *Methods.* 157:28–41.
6. Hennen, J., C. A. Saunders, …, G. W. G. Luxton. 2018. Fluorescence fluctuation spectroscopy reveals differential SUN protein oligomerization in living cells. *Mol. Biol. Cell.* 29:1003–1011.
7. Sosa, B. A., A. Rothballer, …, T. U. Schwartz. 2012. LINC complexes form by binding of three KASH peptides to domain interfaces of trimeric SUN proteins. *Cell.* 149:1035–1047.
8. Jahed, Z., D. Fadavi, …, M. R. K. Mofrad. 2018. Molecular insights into the mechanisms of SUN1 oligomerization in the nuclear envelope. *Biophys. J.* 114:1190–1203.
9. Nie, S., H. Ke, …, W. Feng. 2016. Coiled-coil domains of SUN proteins as intrinsic dynamic regulators. *Structure.* 24:80–91.
10. Zhou, Z., X. Du, …, Q. Wang. 2012. Structure of Sad1-UNC84 homology (SUN) domain defines features of molecular bridge in nuclear envelope. *J. Biol. Chem.* 287:5317–5326.
11. Yogurtcu, O. N., and M. E. Johnson. 2018. Cytosolic proteins can exploit membrane localization to trigger functional assembly. *PLoS Comput. Biol.* 14:e1006031.
12. Lv, Z., M. Hashemi, …, Y. L. Lyubchenko. 2019. Assembly of α-synuclein aggregates on phospholipid bilayers. *Biochim. Biophys. Acta. Proteins Proteomics.* 1867:802–812.
13. Smith, E. M., J. Hennen, …, J. D. Mueller. 2015. Z-scan fluorescence profile deconvolution of cytosolic and membrane-associated protein populations. *Anal. Biochem.* 480:11–20.
14. Smoyer, C. J., S. S. Katta, …, S. L. Jaspersen. 2016. Analysis of membrane proteins localizing to the inner nuclear envelope in living cells. *J. Cell Biol.* 215:575–590.
15. Ruan, Q., Y. Chen, …, W. W. Mantulin. 2002. Cellular characterization of adenylate kinase and its isoform: two-photon excitation fluorescence imaging and fluorescence correlation spectroscopy. *Biophys. J.* 83:3177–3187.
16. Saunders, C. A., N. J. Harris, …, G. W. G. Luxton. 2017. TorsinA controls TAN line assembly and the retrograde flow of dorsal perinuclear

actin cables during rearward nuclear movement. *J. Cell Biol.* 216:657–674.

17. Thaler, C., S. V. Koushik, …, S. S. Vogel. 2009. Structural rearrangement of CaMKIIalpha catalytic domains encodes activation. *Proc. Natl. Acad. Sci. USA.* 106:6369–6374.
18. Zacharias, D. A., J. D. Violin, …, R. Y. Tsien. 2002. Partitioning of lipid-modified monomeric GFPs into membrane microdomains of live cells. *Science.* 296:913–916.
19. Vander Heyden, A. B., T. V. Naismith, …, P. I. Hanson. 2011. Static retention of the lumenal monotopic membrane protein torsinA in the endoplasmic reticulum. *EMBO J.* 30:3217–3231.
20. Hennen, J., K. H. Hur, …, J. D. Mueller. 2020. Identifying hetero-protein complexes in the nuclear envelope. *Biophys. J.* 118:26–35, Published online November 22, 2019.
21. Smith, E. M., P. J. Macdonald, …, J. D. Mueller. 2014. Quantifying protein-protein interactions of peripheral membrane proteins by fluorescence brightness analysis. *Biophys. J.* 107:66–75.
22. Hennen, J., I. Angert, …, J. D. Mueller. 2018. Investigating LINC complex protein homo-oligomerization in the nuclear envelopes of living cells using fluorescence fluctuation spectroscopy. *Methods Mol. Biol.* 1840:121–135.
23. Chen, Y., L.-N. Wei, and J. D. Müller. 2003. Probing protein oligomerization in living cells with fluorescence fluctuation spectroscopy. *Proc. Natl. Acad. Sci. USA.* 100:15492–15497.
24. Hennen, J., K. H. Hur, and J. D. Mueller. 2019. Quantitative modeling of self-oligomerization of proteins in the nuclear envelope by fluorescence fluctuation analysis. *Anal. Biochem.* 582:113359.
25. Karuka, S. R., J. Hennen, …, J. D. Mueller. 2019. Time-shifted mean-segmented Q data of a luminal protein measured at the nuclear envelope by fluorescence fluctuation microscopy. *Data Brief.* 28:105005.
26. Wu, B., Y. Chen, and J. D. Müller. 2009. Fluorescence fluctuation spectroscopy of mCherry in living cells. *Biophys. J.* 96:2391–2404.
27. Lin, B., J. Yu, and S. A. Rice. 2000. Direct measurements of constrained brownian motion of an isolated sphere between two walls. *Phys. Rev. E Stat. Phys. Plasmas Fluids Relat. Interdiscip. Topics.* 62:3909–3919.
28. Hink, M. A., R. A. Griep, …, A. J. Visser. 2000. Structural dynamics of green fluorescent protein alone and fused with a single chain Fv protein. *J. Biol. Chem.* 275:17556–17560.
29. Callan, A. C., S. Bunning, …, E. Swanton. 2007. Biosynthesis of the dystonia-associated AAA+ ATPase torsinA at the endoplasmic reticulum. *Biochem. J.* 401:607–612.
30. Korson, L., W. Drost-Hansen, and F. J. Millero. 1969. Viscosity of water at various temperatures. *J. Phys. Chem.* 73:34–39.
31. Bag, N., D. H. X. Yap, and T. Wohland. 2014. Temperature dependence of diffusion in model and live cell membranes characterized by imaging fluorescence correlation spectroscopy. *Biochim. Biophys. Acta.* 1838:802–813.
32. Naismith, T. V., J. E. Heuser, …, P. I. Hanson. 2004. TorsinA in the nuclear envelope. *Proc. Natl. Acad. Sci. USA.* 101:7612–7617.
33. Qian, H., and E. L. Elson. 1990. On the analysis of high order moments of fluorescence fluctuations. *Biophys. J.* 57:375–380.
34. Ostlund, C., E. S. Folker, …, H. J. Worman. 2009. Dynamics and molecular interactions of linker of nucleoskeleton and cytoskeleton (LINC) complex proteins. *J. Cell Sci.* 122:4099–4108.
35. Michael, D. J., X. Geng, …, R. H. Chow. 2004. Fluorescent cargo proteins in pancreatic beta-cells: design determines secretion kinetics at exocytosis. *Biophys. J.* 87:L03–L05.
36. Schornack, S., R. Fuchs, …, S. Kamoun. 2009. Protein mislocalization in plant cells using a GFP-binding chromobody. *Plant J.* 60:744–754.
37. Goodchild, R. E., A. L. Buchwalter, …, P. I. Hanson. 2015. Access of torsinA to the inner nuclear membrane is activity dependent and regulated in the endoplasmic reticulum. *J. Cell Sci.* 128:2854–2865.
38. Goodchild, R. E., and W. T. Dauer. 2004. Mislocalization to the nuclear envelope: an effect of the dystonia-causing torsinA mutation. *Proc. Natl. Acad. Sci. USA.* 101:847–852.